Supporting Information

Robust, Tough, Ultra-Low Creep and Reproessable Rubber Enabled by Weak Supramolecular Interactions-Dominated Yet Strong Covalent Bonds-Assisted Reverse Design Paradigm

Wei-Chen Zhou[1, 2, 3], Xue-Qin Gao [3]*, Jia-Hao Li [2, 3], Chen Ye [2, 5], Yu-Zhong Wang[1, 2, 5], and Cong Deng [2, 4]*

1- State Key Laboratory of Polymer Materials Engineering, Sichuan University, Chengdu 610065, People's Republic of China

2- Collaborative Innovation Center for Eco-Friendly and Fire-Safety Polymeric Materials (MoE), National Engineering Laboratory for Eco-Friendly Polymer Materials (Sichuan), Sichuan University, Chengdu 610064, People's Republic of China

3- College of Polymer Science and Engineering, Sichuan University, Chengdu 610065, People's Republic of China

4- Analytical & Testing Center, Sichuan University, Chengdu 610064, People's Republic of China

5- College of Chemistry, Sichuan University, Chengdu 610064, People's Republic of China

E-mail addresses: dengcong@scu.edu.cn (C. Deng), gaoxueqin@scu.edu.cn (X.-Q. Gao)

This PDF file includes:

Experimental Section

Materials

ENR-50 (epoxidation degree of 50%, M_n=100178, polymer dispersity index=2.196) was purchased from the Agricultural Products Processing Research Institute, China. 4-Formylbenzoic acid (pFBA, 98%), 4,4'-diaminodiphenyl disulfide (APDS, 98%), anhydrous zinc acetate ($Zn(OAc)_2$, 99.99%) and 1,2-dimethylimidazole (DMI, 98%) were purchased from Aladdin Ltd, China. Anhydrous ethanol (EtOH, 99%) was purchased from Kelong Co., Ltd, China.

Synthesis of Diacids Containing Schiff Bases and Disulfides (Sch-2S)

The dynamic crosslinking agent Sch-2S, which incorporates Schiff base and disulfides, was synthesized through an amine-aldehyde condensation reaction. Initially, 0.12 mol of pFBA was introduced into a three-necked flask containing ethanol under a nitrogen atmosphere and refluxed at 80 °C until complete dissolution. Subsequently, an ethanol solution of APDS was added dropwise to the flask, and the reaction was allowed to proceed. Upon completion, the mixture underwent hot filtration followed by three washes with hot ethanol. Finally, the product Sch-2S was obtained by drying at 80°C in a vacuum oven for 12 hours.

Prepare of Hybrid Crosslinked ENR (HC-ENR)

ENR-50, $Zn(OAc)_2$, Sch-2S, and DMI were mixed via two-roll milling. Subsequently, curing was conducted by compression molding at a temperature of 180°C, pressure of 10 MPa, and curing time determined from the vulcanization curve. For the HC-ENR samples, $Zn(OAc)_2$ was fixed at 10 phr, and the molar ratio of carboxyl groups to oxirane rings was varied as 0, 1/280, 1/210, 1/140, and 1/70. DMI served as a reaction promoter for the carboxyl groups and oxirane rings[1, 2], with the molar ratio adjusted accordingly. In this study, samples were designated as HC-ENR-x, where x denotes the molar ratio of carboxyl groups to oxirane rings. **Fig. S1** indicates that the initial thermal decomposition temperature of Sch-2S is 220 °C, which exceeds the processing

temperature of HC-ENR (180 °C). Therefore, it is believed that Sch-2S meets the processing requirement of HC-ENR.

Characterizations

Proton nuclear magnetic resonance (^{1}H-NMR) spectra were obtained with an AVANCE III HD 400 MHz instrument (Bruker, Germany) at room temperature, employing DMSO-d6 as the solvent and TMS as the internal standard. Fourier transform infrared (FTIR) spectra were recorded on a Nicolet 6700 instrument (Thermo Fisher Scientific, USA), spanning a wavenumber range of 4000-400 cm^{-1}. Vulcanization curves were measured using an RPA8000 Rubber Processing Analyzer (GOTECH, Taiwan) at a vulcanization temperature of 180 °C. Dynamic mechanical analysis (DMA) was performed with a Q850 Dynamic Mechanical Analyzer (TA, USA) in tensile mode. The samples, with a thickness of 0.5 mm, were tested at a frequency of 1 Hz, an amplitude of 15 μm, and a temperature range of -50 to 100 °C, at a heating rate of 3 °C/min. The mechanical properties were evaluated using a Model 5576 Universal Testing Machine (INSTRON, USA), following the GB/T 528-2009 standard. The tests were conducted at room temperature with a tensile rate of 500 mm/min, utilizing dumbbell-shaped specimens with dimensions of 18 mm (length) × 4 mm (width) × 1 mm (thickness). Cyclic tensile tests were also performed under the same conditions, at a rate of 100 mm/min. The reprocessing procedure for sample preparation adhered to established protocols reported in the literature[3]. Rheological properties were assessed using a Discovery HR-2 Dynamic Rheometer (TA, USA) at 25 °C. The samples, circular in shape with a diameter of 25 mm and a thickness of 1 mm, were subjected to strain sweep tests at a shear rate of 1 Hz and frequency sweep tests at a shear strain of 1%. Stress relaxation and creep tests were conducted with the Q850 Dynamic Mechanical Analyzer (TA, USA) in tensile mode. For the stress relaxation tests, a fixed strain of 3% was applied, while for the creep tests, a fixed stress of 0.35 MPa was applied at 80 °C. The sample thickness for these tests was 0.5 mm. The oil immersion test was conducted following the GB/T 1690-2010 standard. Samples of 5 mm (length) × 5 mm (width) × 1 mm (thickness) were immersed in two different commercial engine

oils at room temperature for seven days, with the percentage mass change before and after immersion serving as the indicator of oil resistance. For gas barrier performance, a Labthink C130 gas permeability tester was used, with circular samples of 25 mm in diameter and oxygen as the test gas. The high and low-pressure chambers were degassed for 15 hours, and testing was conducted at a pressure ratio of 10%, with the high-pressure chamber maintained at 101 kPa and the temperature at 23.0°C. For comparing, using sulfur-cured ENR (ENR-S) as a control.

Density Functional Theory (DFT) Calculations

All DFT calculations were performed using the Gaussian 09[4]. In the DFT calculations, geometry optimization was conducted at the B3LYP/def2-SVP level of theory, which were dispersion corrected by D3BJ[5-7] Vibrational frequency analysis was carried out to identify the nature of each stationary points as a minimum state. The solvent effect of water was evaluated by the IEFPCM solvation model. The single point calculations for the optimized geometries were performed to obtain accurate energies at the B3LYP/def2-TZVP level of theory, which were dispersion corrected by D3BJ.

Supplementary Figures

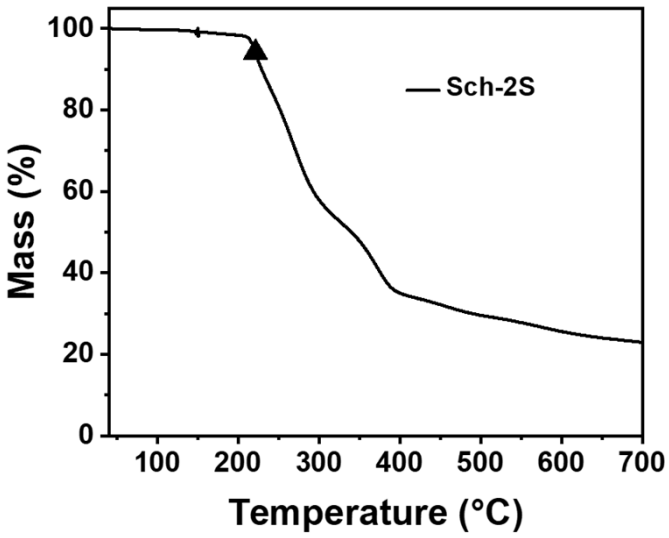

Fig. S1 Thermal decomposition curve of Sch-2S under nitrogen.

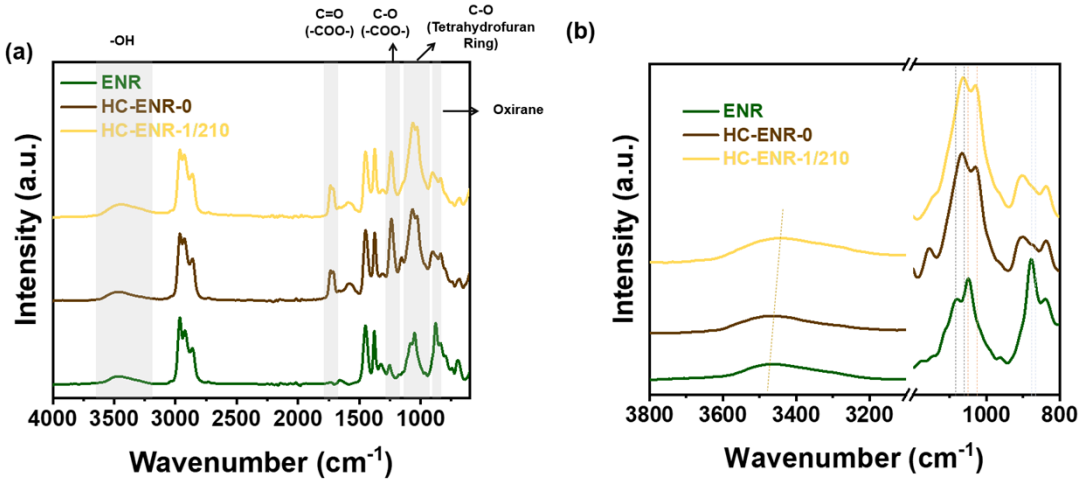

Fig. S2 The FTIR spectra of ENR and HC-ENR.

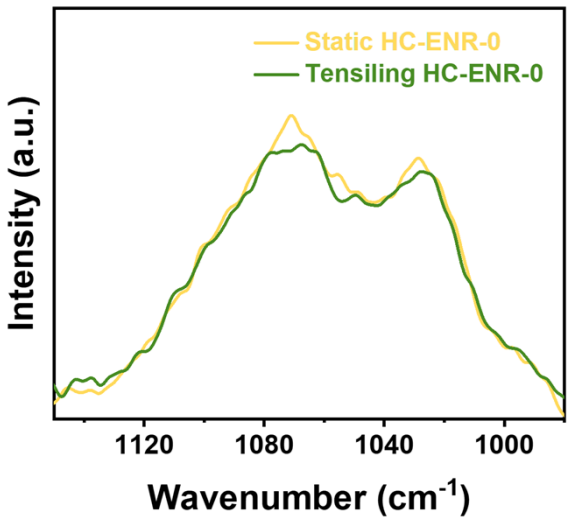

Fig. S3 The FTIR spectra of static and tensiling HC-ENR-0.

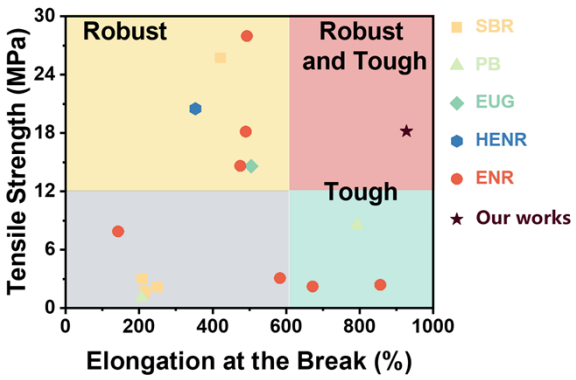

Fig. S4 Comparison of tensile strength and elongation at break between this work and other reprocessable rubbers.

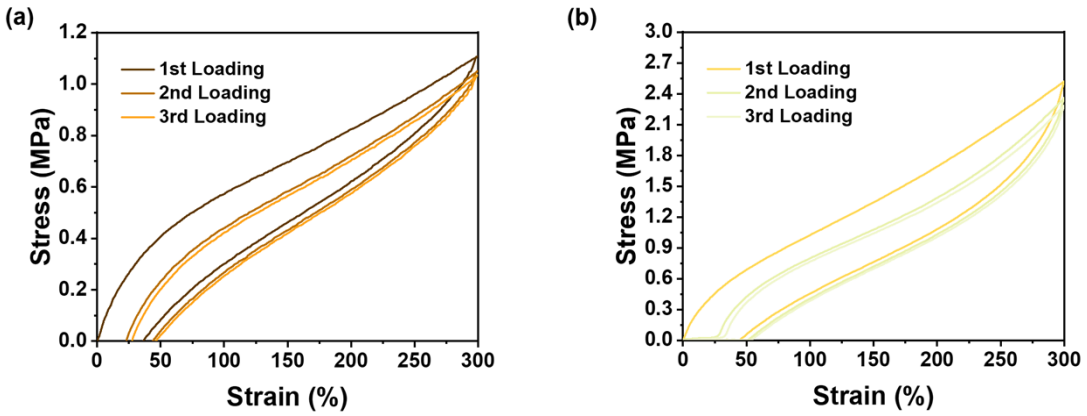

Fig. S5 (a) The cyclic tensile curve of HC-ENR-0. **(b)** The cyclic tensile curve of HC-ENR-1/210.

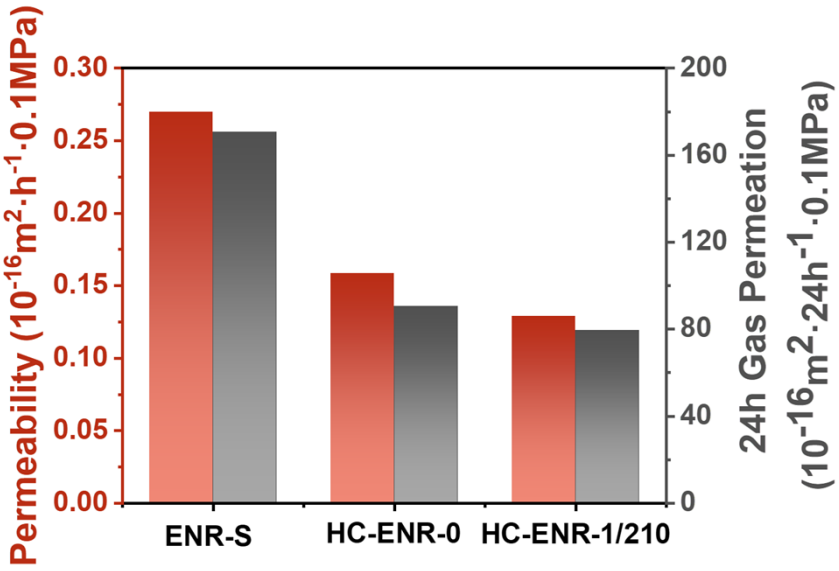

Fig. S6 The gas barrier properties of HC-ENR.

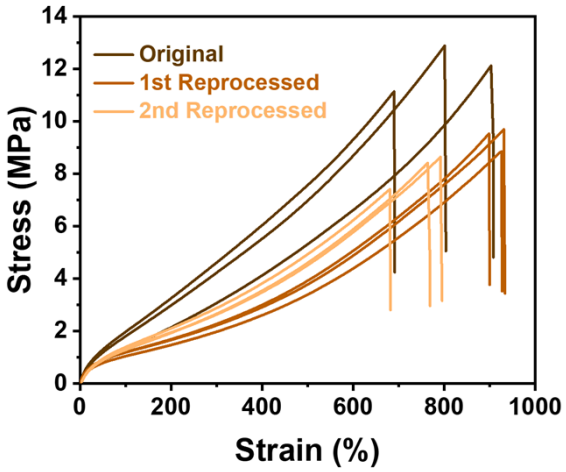

Fig. S7 The stress-strain curves of HC-ENR-0 before and after reprocessing.

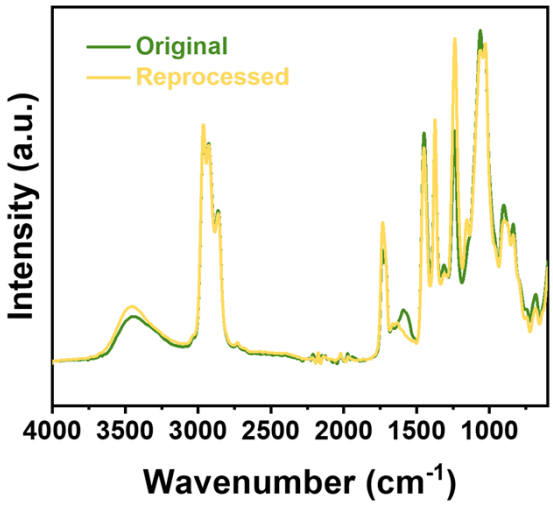

Fig. S8 The FTIR spectra of HC-ENR-0 before and after reprocessing.

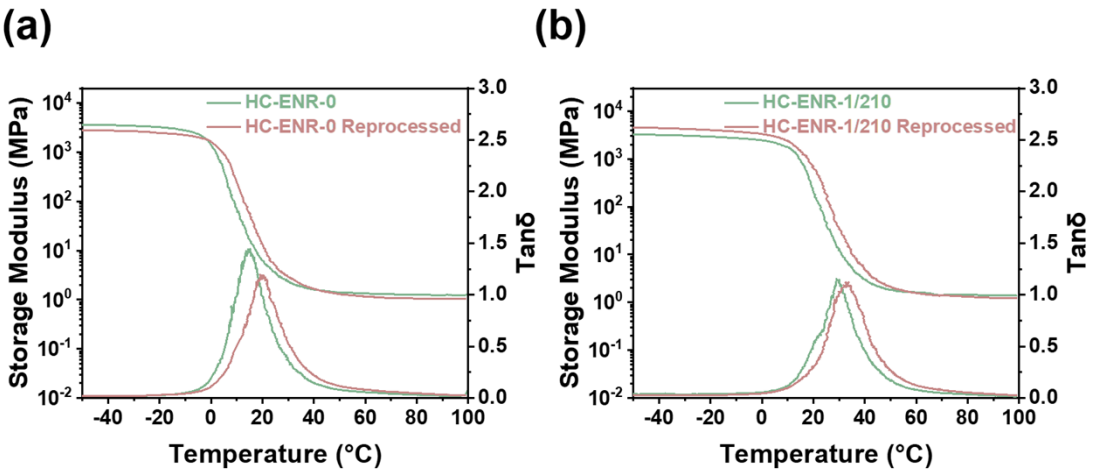

Fig. S9 The DMA curves of **(a)** HC-ENR-0 and **(b)** HC-ENR-0 before and after reprocessing.

After reprocessing, both sets of samples exhibit a notable reduction in the rubber plateau modulus, along with a shift of the Tan δ peak towards higher temperatures and a decrease in peak intensity. We attribute this phenomenon to two primary factors: First, during reprocessing, the formation of additional hydroxyl groups from the oxirane rings fosters hydrogen bonding interactions among these hydroxyls, as well as interactions between the hydroxyl groups and Zn^{2+} ions. These interactions remain relatively stable at lower temperatures, thereby inhibiting the slip of rubber chain segments. Second, the consumption of oxirane rings leads to a weakening of the stronger Zn^{2+}-O coordination interactions within the rubber matrix, resulting in a decrease in modulus at elevated temperatures.

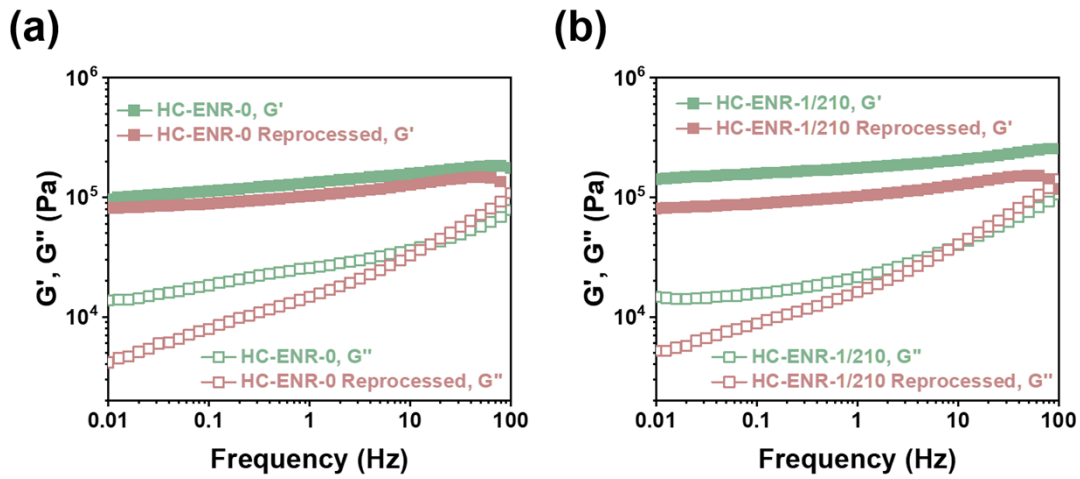

Fig. S10 The frequency strain sweep curves of **(a)** HC-ENR-0 and **(b)** HC-ENR-0 before and after reprocessing.

The storage modulus of the rubber decreases after reprocessing, aligning with our previous analysis concerning the depletion of oxirane rings, which diminishes the strong Zn^{2+}-O coordination interactions. Furthermore, it is important to highlight that the reprocessed samples exhibit a higher loss modulus (G") at shorter observation scales (high frequency), indicating an increase in weak physical interactions within HC-ENR-1/210. In contrast, the significant reduction in loss modulus observed in the low-frequency region similarly reflects the weakening of the strong Zn^{2+}-O coordination interactions.

Supplementary Tables

Table S1 Comparison of mechanical properties between this work and other reprocessable rubbers.

Rubber	Strength (MPa)	Elongation at Break (%)	Toughness (MJ/m^3)	Ref
SBR[a]	2.17	~250	/	8
	25.7	421	43.1	9
	3	208	3.15	10
	1.7	217	/	11
PB[b]	1.08	207	/	12
	8.57	793	39.12	13
EUG[c]	14.6	505	38.1	14
	10.4	856	34.2	14
HENR[d]	20.5	353	32	15
ENR[e]	14.63	475	/	16
	16.56	776	56.9	17
	18.15	~490	23.8	18
	27.97	493	40.2	18
	3.1	583	/	19
	7.9	143	/	20
	2.40	856	9.47	21
	2.23	672	/	22
	18.18	**927**	**74.34**	**Our Work**

Table S2 Oil resistance of HC-ENR

	Sample	Mass before Immersion (g)	Mass after Immersion (g)	Mass Varieties Percent (%)
Commercial Engine Oil-1	ENR-S	0.0873	0.0891	2.06
	HC-ENR-0	0.0798	0.0809	1.38
	HC-ENR-1/210	0.0622	0.0629	1.13
Commercial Engine Oil-2	ENR-S	0.0833	0.0846	1.56
	HC-ENR-0	0.0989	0.1002	1.32
	HC-ENR-1/210	0.0668	0.0675	1.05

Table S3 Characteristic relaxation times of HC-ENR at different temperatures.

Temperature (°C)	Relaxation Time of HC-ENR-0 (s)	Relaxation Time of HC-ENR-1/210 (s)
110	11248	5722
120	5625	3612
130	3864	2613
140	2188	1616

Table S4 Comparison of mechanical properties of rubbers after reprocessing between this work and other reprocessable rubbers.

Rubber	Strength (MPa)	Elongation at Break (%)	Ref
SBR	2.08	218	8
	~15	~320	9
	~2.6	~230	11
PB	~0.9	~160	12
	~8.5	~700	13
EUG	9.57	736	14
HENR	15.38	282	15
ENR	~12.5	~450	16
	~12.8	~610	17
	~14.8	~450	18
	~15	~430	18
	~1.2	~500	19
	~7	~144	20
	~2.6	~840	21
	~1.94	~550	22
	11.84	**954**	**Our Work**

Table S5 Comparison of creep rate at 80 °C between this work and other reprocessable rubbers.

Rubber	**Stress (MPa)**	**Creep Rate (%/min)**	Ref
SBR	0.10	0.0617	9
	0.25	0.00187	11
PDMS[f]	0.001	0.0066	23
	0.1	0.03	24
PI[g]	0.2	0.013	25
	0.01	0.297	26
LCE[l]	0.25	0.126	27
HNBR[m]	0.10	0.011	28
ENR	**0.35**	**0.00024**	**Our Work**

Abbreviations:

SBR[a]-Styrene-butadiene rubber;

PB[b]-Polybutadiene;

EUG[c]-Eucommia ulmoides gum;

HENR[d]-Hydroxylated epoxidized natural rubber;

ENR[e]-Epoxidized natural rubber;

PDMS[f]-Polydimethylsiloxane;

PI[g]-Polyisoprene;

LCE[l]-Liquid crystal elastomers;

HNBR[m]-Hydrogenated nitrile butadiene rubber.

References

1. M. Pire, S. Norvez, I. Iliopoulos, B. Le Rossignol and L. Leibler, *Polymer*, 2011, **52**, 5243-5249.
2. M. Pire, C. Lorthioir, E. K. Oikonomou, S. Norvez, I. Iliopoulos, B. Le Rossignol and L. Leibler, *Polymer Chemistry*, 2012, **3**, 946-953.
3. W. Song, Z. Wang, Y. Xing, G. Zhang, X. Zhang, Y. Lu, T. Tan and L. Zhang, *ACS Sustainable Chemistry & Engineering*, 2023, **11**, 2784-2796.
4. G. W. T. M. J. Frisch, H. B. Schlegel, G. E. Scuseria, M. A. Robb, J. R. Cheeseman, G. Scalmani, V. Barone, B. Mennucci, G. A. Petersson, H. Nakatsuji, M. Caricato, X. Li, H. P. Hratchian, A. F. Izmaylov, J. Bloino, G. Zheng, J. L. Sonnenberg, M. Hada, M. Ehara, K. Toyota, R. Fukuda, J. Hasegawa, M. Ishida, T. Nakajima, Y. Honda, O. Kitao, H. Nakai, T. Vreven, J. A. Montgomery, Jr., J. E. Peralta, F. Ogliaro, M. Bearpark, J. J. Heyd, E. Brothers, K. N. Kudin, V. N. Staroverov, T. Keith, R. Kobayashi, J. Normand, K. Raghavachari, A. Rendell, J. C. Burant, S. S. Iyengar, J. Tomasi, M. Cossi, N. Rega, J. M. Millam, M. Klene, J. E. Knox, J. B. Cross, V. Bakken, C. Adamo, J. Jaramillo, R. Gomperts, R. E. Stratmann, O. Yazyev, A. J. Austin, R. Cammi, C. Pomelli, J. W. Ochterski, R. L. Martin, K. Morokuma, V. G. Zakrzewski, G. A. Voth, P. Salvador, J. J. Dannenberg, S. Dapprich, A. D. Daniels, O. Farkas, J. B. Foresman, J. V. Ortiz, J. Cioslowski, D. J. Fox, *Gaussian 09, Version D.01, Gaussian, Inc., Wallingford CT, 2013*.
5. F. Weigend and R. Ahlrichs, *Physical Chemistry Chemical Physics*, 2005, **7**, 3297-3305.
6. S. Grimme, J. Antony, S. Ehrlich and H. Krieg, *The Journal of Chemical Physics*, 2010, **132**, 154104.
7. S. Grimme, S. Ehrlich and L. Goerigk, *Journal of Computational Chemistry*, 2011, **32**, 1456-1465.
8. Y. Chen, Z. Tang, X. Zhang, Y. Liu, S. Wu and B. Guo, *ACS Applied Materials & Interfaces*, 2018, **10**, 24224-24231.
9. Y. Liu, Z. Tang, D. Wang, S. Wu and B. Guo, *Journal of Materials Chemistry A*, 2019, **7**, 26867-26876.
10. L. Wang, Y. Liu, N. Hao, Y. Qiao, W. Zeng, L. Wei and A. Du, *Polymer*, 2023, **265**, 125595.
11. X. Li, S. Wu, S. Yu, C. Xiao, Z. Tang and B. Guo, *Polymer*, 2022, **238**, 124379.
12. Y. Liu, Z. Tang, J. Chen, J. Xiong, D. Wang, S. Wang, S. Wu and B. Guo, *Polymer Chemistry*, 2020, **11**, 1348-1355.
13. W. Wang, W. Zhang, Z. Liu, Y. Xue, X. Lei, G. Gong and Q. Zhang, *Journal of Materials Chemistry C*, 2021, **9**, 6241-6250.
14. X. Qi, J. Zhang, L. Zhang and D. Yue, *Journal of Materials Chemistry A*, 2021, **9**, 25399-25407.
15. S. Wu, S. Fang, Z. Tang, F. Liu and B. Guo, *Materials & Design*, 2020, **192**, 108756.
16. Y. Chen, Z. Tang, Y. Liu, S. Wu and B. Guo, *Macromolecules*, 2019, **52**, 3805-3812.
17. L. Huang, Y. Yang, Z. Niu, R. Wu, W. Fan, Q. Dai, J. He and C. Bai, *Macromolecular Rapid Communications*, 2021, **42**, 2100432.
18. Y. Liu, Z. Tang, S. Wu and B. Guo, *ACS Macro Letters*, 2019, **8**, 193-199.
19. W. Liu, J. Huang, Z. Gong, J. Fan and Y. Chen, *Polymer*, 2022, **252**, 124900.
20. H. Dong, G. Zhang and Y. Zhang, *Composites Science and Technology*, 2023, **238**, 110025.
21. J. Huang, Z. Gong and Y. Chen, *Polymer*, 2022, **242**, 124569.
22. L. Cao, Z. Gong, C. Liu, J. Fan and Y. Chen, *Composites Science and Technology*, 2021, **207**, 108750.
23. Y. Spiesschaert, M. Guerre, L. Imbernon, J. M. Winne and F. Du Prez, *Polymer*, 2019, **172**, 239-246.

24. H. Zhang, C. Cai, W. Liu, D. Li, J. Zhang, N. Zhao and J. Xu, *Scientific Reports*, 2017, **7**, 11833.
25. L. Huang, Y. Yang, R. Wu, W. Fan, Q. Dai, J. He and C. Bai, *Polymer*, 2020, **208**, 122964.
26. A. Breuillac, F. Caffy, T. Vialon and R. Nicolaÿ, *Polymer Chemistry*, 2020, **11**, 6479-6491.
27. D. W. Hanzon, N. A. Traugutt, M. K. McBride, C. N. Bowman, C. M. Yakacki and K. Yu, *Soft Matter*, 2018, **14**, 951-960.
28. S. Kaiser, S. Wurzer, G. Pilz, W. Kern and S. Schlögl, *Soft Matter*, 2019, **15**, 6062-6072.